molecules

MDPI

Article

Ferrocenophanium Stability and Catalysis

Sai Anvesh Bezawada, Neira Ušto, Chloe Wilke, Michael Barnes-Flaspoler, Rajamoni Jagan and Eike B. Bauer *

Department of Chemistry and Biochemistry, University of Missouri, One University Boulevard, St. Louis, MO 63121, USA
* Correspondence: bauere@umsl.edu; Tel.: +1-(314)-516-5311; Fax: +1-(314)-516-5342

Abstract: Ferrocenium catalysis is a vibrant research area, and an increasing number of ferrocenium-catalyzed processes have been reported in the recent years. However, the ferrocenium cation is not very stable in solution, which may potentially hamper catalytic applications. In an effort to stabilize ferrocenium-type architectures by inserting a bridge between the cyclopentadienyl rings, we investigated two ferrocenophanium (or *ansa*-ferrocenium) cations with respect to their stability and catalytic activity in propargylic substitution reactions. One of the ferrocenophanium complexes was characterized by single crystal X-ray diffraction. Cyclic voltammetry experiments of the ferrocenophane parent compounds were performed in the absence and presence of alcohol nucleophiles, and the stability of the cations in solution was judged based on the reversibility of the electron transfer. The experiments revealed a moderate stabilizing effect of the bridge, albeit the effect is not very pronounced or straightforward. Catalytic propargylic substitution test reactions revealed decreased activity of the ferrocenophanium cations compared to the ferrocenium cation. It appears that the somewhat stabilized ferrocenophanium cations show decreased catalytic activity.

Keywords: ferrocenophanium cations; catalyst stability; propargylic substitution reactions

Citation: Bezawada, S.A.; Ušto, N.; Wilke, C.; Barnes-Flaspoler, M.; Jagan, R.; Bauer, E.B. Ferrocenophanium Stability and Catalysis. *Molecules* **2023**, *28*, 2729. https://doi.org/10.3390/molecules28062729

Academic Editors: Maria Luisa Di Gioia, Luísa Margarida Martins and Isidro M. Pastor

Received: 22 February 2023
Revised: 8 March 2023
Accepted: 9 March 2023
Published: 17 March 2023

1. Introduction

In recent years, there has been an increasing interest in catalytic processes based on 3d transition metals, which are abundant and relatively inexpensive [1]. Consequently, like with other 3d transition metals, iron catalysis has emerged as a vibrant research area in the past decades [2–17]. Iron-based catalysis has a number of advantages compared to other transition metals typically utilized in catalysis. It is relatively non-toxic, abundant, inexpensive, and environmentally benign. Accordingly, several organic transformations have been reported to be catalyzed by iron-based catalyst systems, such as oxidations, reductions, substitutions, cross-coupling, or polymerization reactions. Iron-based catalysts can range from simple salts like FeX_2 or FeX_3 [18–20], $Fe(OTf)_2$ [21,22], $Fe(OAc)_2$ [23–26], or $Fe(acac)_3$ (acac = acetylacetonato) [27] to higher-sophisticated metal complexes such as Knölker's or related complexes [28,29], iron complexes derived from phosphorus- [7,30] or nitrogen-coordinating ligands [31,32] or iron coordination compounds which can catalyze reactions site- or substrate-selectively [33–35] and enantioselectively [36–38].

We have employed a number of iron-based catalysts in the past in oxidation reactions [39–45], and during the course of our studies, we found that ferrocenium hexafluorophosphate ($FcPF_6$) catalyzes propargylic substitution reactions [46,47]. Ferrocenium cations have been increasingly applied as catalysts in a number of other reactions [48], such as Friedel-Crafts [49,50] and allylic alkylations [51], amine [52] or CH oxidations [53], cyanosilylation of carbonyl compounds [54], reductive etherification [55], aminolysis [56] or ring opening of epoxides [57], aromatic iodinations [58], the Strecker reaction [59], the Mannich reaction [60], photodecomposition [61], ring expansion [62], or polymerization reactions [63–66]. Antiproliferative effects of certain ferrocenophanes have been reported [67]. The tunability of the ferrocenium platform provides an advantage when it comes to catalyst improvement.

However, ferrocenium cations are not very stable in solution, especially in chlorinated solvents and under aerobic conditions [68–73]. The ferrocenium cation decomposes in solution, and this fact has also been taken advantage of in Diels-Alder reactions [73]. Catalyst decomposition is a big concern, as it may counter efforts to design catalysts for specific purposes. As such, efforts to investigate catalyst decomposition and the design of more robust catalyst systems are important issues.

Herein, we investigate ferrocenophanium cations as potentially more stable complexes compared to ferrocenium and test them as catalysts in propargylic substitution reactions. Ferrocenophanes (or *ansa*-ferrocenes) are ferrocene complexes, where the two cyclopentadienyl (Cp) ring systems are bridged (e.g., **1** and **2** in Scheme 1, top). We hypothesized that a bridge between the Cp rings stabilizes the complex, and would slow down or block decomposition pathways, such as decomposition by Cp ring loss or intermolecular decomposition by nucleophilic attack on the iron (which would in a ferrocenophane be somewhat protected by the bridge). We determined the stability of ferrocenophanium cations in the absence and presence of nucleophiles by cyclic voltammetry, and we applied the cations in propargylic substitution test reactions (Scheme 1, bottom).

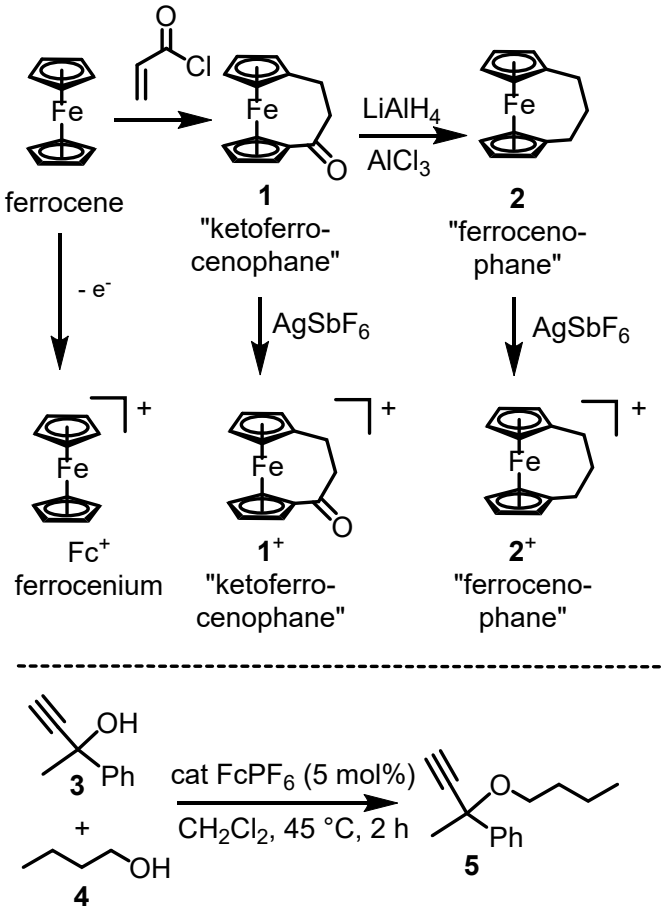

Scheme 1. Ferrocene and ferrocenophanium complexes and catalytic application.

2. Results and Discussion

Ferrocenophanes or *ansa*-ferrocenes are a well-known compound class [74]. The bridges can be all-carbon [74,75] or contain heteroatoms [76,77], and several synthetic methods for their access have been described [78]. Either the two ring systems are connected by a series of organic transformations, or a preformed, bidentate dicyclopentadienyl ligand is coordinated to an iron center ("flytrap method") [79]. We set out to synthesize and investigate the known, mono-bridged "ketoferrocenophane" complex **1**, which can be obtained from ferrocene in an acylation-Michael reaction sequence (Scheme 1) [80,81]. The keto

functionality can be reduced to obtain the hydrocarbon-only bridge in the "ferrocenophane" **2** (Scheme 1) [80,81]. The chemistry to obtain ferrocenophanes **1** and **2** worked as described in the literature. The conversion from **1** to **2** can be followed by IR, as the C=O stretch in **1** disappears after reduction. However, the workup procedures are tedious, and the yields are generally not very high, as also indicated in the original synthetic procedures. Oxidation of the two complexes led to the corresponding ferrocenophanium salts $\mathbf{1}^{+}SbF_6$ [82] and $\mathbf{2}^{+}SbF_6$ [83,84]. The oxidation of **1** and **2** can be observed by UV-vis spectroscopy, as $\mathbf{1}^{+}SbF_6$ and $\mathbf{2}^{+}SbF_6$ give a new band around 620 nm, as it is characteristic of ferrocenophanium cations [83]. NMR investigation of the ferrocenophanium salts is, due to their paramagnetic nature, not possible. Consequently, our investigations were plagued by difficulties accessing the ferrocenophanium ions in large quantities.

The molecular structure of $\mathbf{1}^{+}SbF_6^{-}$ determined by single crystal X-ray diffraction analysis is shown in Figure 1. The details of intensity data collection and refinement are given in the Supporting Information. The crystal structure refinement parameters are summarized in Table 1.

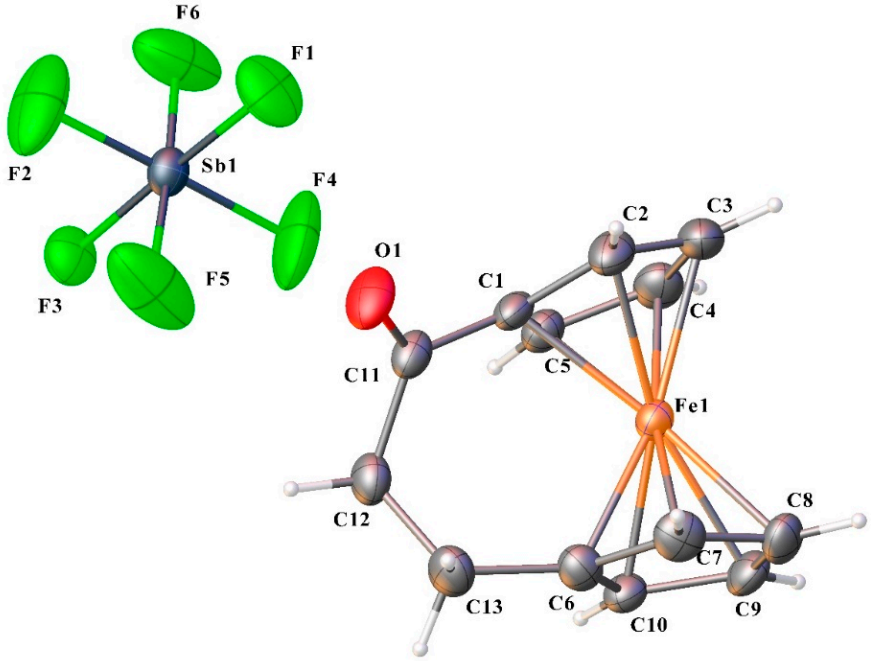

Figure 1. Molecular structure of $\mathbf{1}^{+}SbF_6$ showing the displacement ellipsoids drawn at 50% probability level with atom labeling scheme. Key bond lengths (Å) and angles (°): C(1)-Fe(1): 2.033(10), C(6)-Fe(1): 2.026(13), C(11)-O(1):1.219(13), Cp(centroid)-Fe: 1.693; Cp-Cp angle: 14.39(6), C11-C12-C13: 111.0(11).

The complex $\mathbf{1}^{+}SbF_6$ crystallizes in monoclinic spacegroup P21/c with one ferrocenophanium complex and one SbF_6^{-} anion in the asymmetric unit. From the crystal structure it is observed that the monosubstituted C_5H_4 rings are η^5 coordinated to the central iron atom with C(Cp)-Fe bond lengths ranging from 2.020(6) Å to 2.127(8) Å, showing a significant range. The short C(Cp)-Fe bond length values such as C1(Cp)-Fe1 = 2.020(6) Å and C6(Cp)-Fe1 = 2.040(9) Å is attributed to the substitutions at C1 and C6 positions, respectively. The metallocene conformation is eclipsed with a slightly distorted ferrocene framework showing a Cp(centroid)-Fe-Cp(centroid) angle of 171.8(2)° and Cp(centroid)-Fe distance of 1.692(5) Å and 1.6939(13) Å respectively. The carbonyl group is trigonally planar with the C1-C11-C12 [117.4(6)°] angle being slightly smaller than C1-C11-O1 [121.2(9)°] and O1-C11-C12 [120.9(9)°], respectively. Interestingly, the trigonal planar carbonyl group is oriented out of the adjacent Cp-planes with calculated dihedral angles of 41.56(3)° and 51.44(3)°, respectively. In the SbF_6^{-} anions, the bond lengths and angles are within the expected range with Sb-F distances ranging from 1.771(11) Å to 1.878(5) Å. In the three-dimensional crystal structure, the molecules are mainly stabilized by C-H...O and C-H...F interactions

(Supporting Information Table S1). The oxygen atom O1 acts as a bifurcated acceptor forming two C-H ... O interactions such as C10-H10...O1 and C12-H12A...O1 which connects the adjacent ferrocenophanium complexes (Supplementary Materials, Figure S1). Adjacent ferrocenophanium chains are further bridged by SbF_6^- anions via three C-H...F interactions (C3-H3...F3, C5-H5...F1, and C7-H7...F3), which results in the formation of a three-dimensional network in the crystalline solid. The interlinkage of the ferrocenophanium complex chain and the SbF_6^- anions via C-H...F interaction is illustrated in Figure S2.

Table 1. Crystal Structure Refinement of $\mathbf{1}^+SbF_6$.

Parameters	Complex $\mathbf{1}^+\mathbf{SbF_6}$
Empirical formula	$C_{13}H_{12}F_6FeOSb$
Formula weight	475.83
Temperature (K)	296.15
Wavelength (Å)	1.54178
Crystal system, space group	Monoclinic, $P2_1/c$
Unit cell dimensions	
a (Å)	7.2292(2)
b (Å)	20.6452(5)
c (Å)	10.7792(3)
α (°)	90
β (°)	107.127(2)
γ (°)	90
Volume ($Å^3$)	1537.43(7)
Z, Calculated density (Mg/m^3)	4, 2.056
Absorption coefficient (mm^{-1})	22.107
F(000)	916.0
Crystal size (mm)	0.08 × 0.050 × 0.020
Theta range for data collection (°)	4.883 to 68.48 deg.
Limiting indices	$-8 \leq h \leq 8, -24 \leq k \leq 24, -12 \leq l \leq 12$
Reflections collected/unique	15701/2821 [R(int) = 0.0815]
Completeness to theta = 68.48 (%)	100.0
Refinement method	Full-matrix least-squares on F^2
Data/restraints/parameters	2821/0/199
Goodness-of-fit on F^2	1.068
Final R indices [I>2sigma(I)]	R1 = 0.0520, wR2 = 0.1482
R indices (all data)	R1 = 0.0706, wR2 = 0.1603
Largest diff. peak and hole ($eÅ^{-3}$)	1.12→nd −1.08

The bridge in the ferrocenophanium cation $\mathbf{1}^+$ causes the Cp rings to be inclined to each other with a dihedral (or tilt) angle of 14.39(6)° (α in Figure 2) [85,86]. Therefore, there is some open space on the opposite side of the bridge, where we hypothesized catalysis can take place. The tilt is smaller compared to ferrocenophanes with bridges consisting of two atoms, where angles around 22° have been reported [87]. Ferrocenophanes with a bridge consisting of only one atom exhibit angles between 27 and 38°, putting a substantial strain on the system [79,88]. Obviously, the shorter the bridge, the larger the tilt. In general, atoms directly bonded to the Cp ligands are located in the plane of the ring system. In ferrocenophanes, these atoms can be bent out of the plane of the Cp ring system and quantified with the dip angle [89]. The dip angle is defined as the deviation of the angle between the centroid of the Cp ring, the ipso-carbon atom, and the first carbon atom of the bridge from the ideal 180° (β in Figure 2) [86,89]. The angles were calculated to be 2.81° (C13) and 9.44° (C11, the C=O carbon). It appears that the C1 carbon of the Cp ring bearing the C=O unit has a slightly higher sp^3 character.

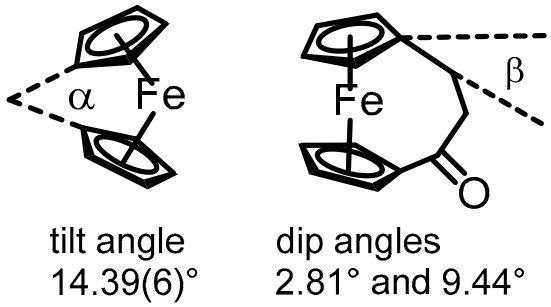

Figure 2. Geometric parameters.

2.1. Cyclic Voltammetry Experiments

We next investigated the stability of the ferrocenophanium cations by cyclic voltammetry (CV) [90,91]. Related experiments have been performed with other ferrocenophanes [92,93]. In a typical CV experiment, the ferrocenophanes are oxidized to the corresponding ferrocenophanium cations. The reversibility of this process, as indicated by the ratio of the i_c/i_a current, would give insight into the stability of $\mathbf{1}^+$ and $\mathbf{2}^+$, compared to the ferrocenium cation. A fully reversible process would give an i_c/i_a ratio of 1. As shown in Scheme 1 (bottom), the catalytic propargylic substitution test reaction involves the propargylic alcohol **3** and *n*-butanol (**4**) as the nucleophile. We also investigated the stability of $\mathbf{1}^+$ and $\mathbf{2}^+$ in the presence of alcohol nucleophiles to investigate whether they are part of potential decomposition chemistry. An i_c/i_a ratio smaller than 1 may indicate an electrochemical oxidation followed by an irreversible chemical reaction (EC mechanism) [91].

Representative CV traces of ferrocene, **1** and **2** in CH_2Cl_2 are shown in Figure 3, in the absence (top) and presence of *n*-BuOH (bottom). As can be seen, all three compounds give the typical "duck-shaped" voltammograms expected for diffusion-controlled, reversible electron-transfer processes [91]. Plots of the peak current i_p versus the square root of the scan rate give linear graphs for diffusion-controlled redox processes [91], which we observed (representative graphs are given in the Supporting Information). The numerical results of the CV experiments are compiled in Tables 2 and 3.

Table 2. Cyclic Voltammetry Values of Various Complexes.

Entry	Compound	$E_{1/2}$/V	ΔE/mV	i_c/i_a	Solvent
1	Ferrocene	0.460 ± 37	143 ± 26	0.97 ± 0.03	CH_2Cl_2
2	Keto-Ferrocenophane (1)	0.604 ± 20	115 ± 12	0.86 ± 0.04	CH_2Cl_2
3	Ferrocenophane (2)	0.318 ± 63	137 ± 21	0.87 ± 0.04	CH_2Cl_2
4	Ferrocene	0.400 ± 94	184 ± 40	0.98 ± 0.02	CH_3CN
5	Keto-Ferrocenophane (1)	0.658 ± 70	327 ± 53	0.89 ± 0.06	CH_3CN
6	Ferrocenophane (2)	0.395 ± 38	106 ± 10	0.94 ± 0.03	CH_3CN

Conditions: glassy carbon working electrode, Pt counter electrode, Ag wire pseudoreference electrode. Solutions 1 mM in substrate, 0.1 M in *n*-Bu_4NPF_6 and flushed with argon. A scan rate of 100 mV s^{-1} was applied and the voltammograms were referenced to ferrocene (E° = 0.46 V in CH_2Cl_2, 0.40 V in CH_3CN).

In Table 2, CV data for ferrocene, and the ferrocenophane complexes **1** and **2** are compiled. This data allows for the comparison of the stability of the ferrocenium cation Fc^+ and the ferrocenophanium complexes $\mathbf{1}^+$ and $\mathbf{2}^+$ in solution in the absence of any other substrate. The ΔE values are a little higher than expected from theory for a reversible electron transfer (59 mV), which may be caused by the poorer conductivity of CH_2Cl_2 and CH_3CN solutions of *n*-Bu_4NPF_6 utilized as the electrolyte; it may also indicate slow electrode kinetics [91]. The ΔE values are somewhat larger in CH_2Cl_2 compared to CH_3CN, which we ascribe to the lower conductivity of CH_2Cl_2, which leads to higher ohmic resistance of the solutions [91]. The complexes are barely soluble in other solvents.

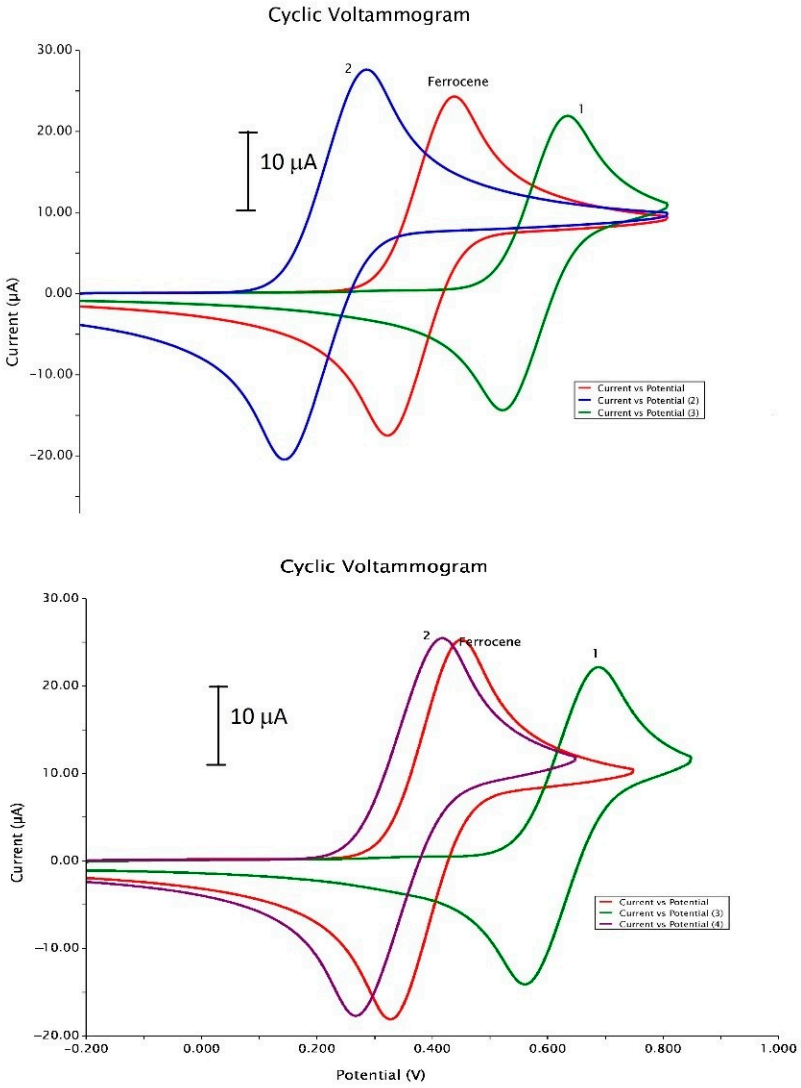

Figure 3. Cyclic voltammograms (scan rate: 100 mV s^{-1}) in CH_2Cl_2 solutions (1.0 mM) at 25 °C (supporting electrolyte *n*-Bu_4NPF_6, 0.1 M), not calibrated. (**Top**): traces from the left **2**, ferrocene, and **1**. (**Bottom**): from the left **2**, ferrocene, and **1** in the presence of *n*-BuOH.

The $E_{1/2}$ values roughly correlate with the oxidation potential of metal complexes. For ferrocene, the standard redox potential is defined as +0.46 V in CH_2Cl_2 and +0.40 V in CH_3CN with *n*-Bu_4NPF_6 as the electrolyte [90]. As derived from the $E_{1/2}$ values, the ketoferrocenophane **1** as a higher oxidation potential of 0.604 V and 0.658 V in CH_2Cl_2 and CH_3CN, respectively (Table 2, entries 2 and 5). These values are higher than that for ferrocene itself, which may be caused by the keto functionality in **1**; it may withdraw electron density from the Cp ring system connected to it, resulting in a higher oxidation potential of the ketoferrocenophane complex **1**. In turn, for ferrocenophane **2**, the redox potentials in CH_2Cl_2 and CH_3CN (+0.318 V and +0.395 V, respectively; entries 3 and 6) are lower than for ferrocene. Here, the electron-donating alkyl bridge may overall increase the electron density of the Cp ring systems, resulting in a lower oxidation potential.

The i_c/i_a ratios allow for the assessment of the stability of the complexes in the solution. If the i_c/i_a ratio is smaller than 1, decomposition of the oxidized species may occur, so that there is less material left after oxidation to be reduced back to the starting material, resulting in a lower reduction current, following an EC mechanism described above [91].

As can be seen, the i_c/i_a ratios for the three complexes are fairly similar, ranging from 0.98 to 0.86 in any solvent. It seems that for the typical timeframe of the CV experiment

(several seconds to minutes, depending on the sweep rate), only a small fraction of the oxidized ferrocene, ketoferrocenophanium $\mathbf{1}^+$, and ferrocenophanium $\mathbf{2}^+$ decompose under the reaction conditions. This behavior may not be unexpected. Ferrocene is known to be fairly stable under CV conditions with fast sweep rates, and it appears that the establishment of a bridge between the Cp rings does not change that significantly during the short time frame of a CV experiment.

Table 3. Cyclic Voltammetry in presence of alcohol nucleophiles.

Entry	Compound	Nucleophile	$E_{1/2}$/V	ΔE/mV	i_c/i_a	Solvent
	Ferrocene					
1		MeOH	0.324 ± 0.043	75 ± 30	0.94 ± 4	CH_3CN
2		*n*-BuOH	0.301 ± 0.047	121 ± 20	0.78 ± 4	CH_3CN
3		*i*-PrOH	0.339 ± 0.021	83 ± 5	0.96 ± 4	CH_3CN
4		Propargylic alcohol **3**	0.410 ± 0.010	117 ± 31	0.88 ± 5	CH_3CN
5		*n*-BuOH	0.404 ± 0.062	128 ± 26	0.94 ± 4	CH_2Cl_2
6		MeOH	0.352 ± 0.041	143 ± 19	0.94 ± 3	CH_2Cl_2
7		*i*-PrOH	0.302 ± 0.080	138 ± 8	0.95 ± 2	CH_2Cl_2
8		Propargylic alcohol **3**	0.344 ± 0.047	145 ± 12	0.94 ± 2	CH_2Cl_2
	Keto-Ferroceno-phane (**1**)					
9		MeOH	0.560 ± 0.032	76 ± 24	0.81 ± 0.04	CH_3CN
10		*n*-BuOH	0.610 ± 0.050	73 ± 20	0.81 ± 0.04	CH_3CN
11		*i*-PrOH	0.590 ± 0.040	72 ± 22	0.82 ± 0.05	CH_3CN
12		Propargylic alcohol **3**				CH_3CN
13		MeOH	0.553 ± 0.078	105 ± 7	0.84 ± 0.06	CH_2Cl_2
14		*n*-BuOH	0.616 ± 0.046	123 ± 23	0.84 ± 0.03	CH_2Cl_2
15		*i*-PrOH	0.432 ± 0.042	117 ± 22	0.87 ± 0.05	CH_2Cl_2
16		Propargylic alcohol **3**	0.648 ± 0.015	109 ± 12	0.75 ± 0.09	CH_2Cl_2
	Ferroceno-phane (**2**)					
17		MeOH	0.233 ± 0.022	75 ± 20	0.97 ± 0.03	CH_3CN
18		*n*-BuOH	0.263 ± 0.048	96 ± 26	0.96 ± 0.04	CH_3CN
19		MeOH	0.288 ± 0.010	108 ± 13	0.96 ± 0.04	CH_2Cl_2
20		*n*-BuOH	0.336 ± 0.007	137 ± 23	0.91 ± 0.02	CH_2Cl_2

Conditions: glassy carbon working electrode, Pt counter electrode, Ag wire pseudoreference electrode at a scan rate of 100 mV s^{-1}. Solutions 1 mM in substrate, 0.1 M in *n*-Bu_4NPF_6 and flushed with argon in presence of the liquid nucleophiles (0.5 mL) or the propargylic alcohol **3** (0.004 g).

However, we were interested to determine how the stability changes in the presence of the catalysis substrates. As mentioned, we applied the ferrocenium cation as a catalyst for propargylic substitution reactions (Scheme 1, bottom), where, besides the catalyst, the tertiary propargylic alcohol **3** and alcohol nucleophiles such as *n*-butanol (**4**), MeOH or *i*-PrOH were present [46,47]. Related CV experiments have been performed by others with ferrocenophanes in the presence of an imidazole base [94]. We performed the same CV experiments as in Table 2 in the presence of propargylic alcohol **3** and a number of primary and secondary aliphatic alcohols. We were interested in whether the stability of the ferrocenophanium complexes changes in the presence of alcohols, as reflected by the i_c/i_a ratios. The results are compiled in Table 3, representative CV traces are shown in Figure 3 (bottom) in the presence of *n*-BuOH. As can be seen, the duck shape is, in general, maintained in the presence of *n*-BuOH.

For ferrocene, the ΔE and the $E_{1/2}$ values are comparable to the measurements in the absence of alcohol. In the presence of MeOH, *i*-PrOH, and the propargylic alcohol **3**, in CH_2Cl_2 or CH_3CN, the ferrocene seems to be fairly stable, as judged by the i_c/i_a ratios, which range from 0.78 to 0.96. In CH_3CN as the solvent, there is a notable difference for *n*-BuOH as the nucleophile. In the presence of *n*-butanol, the i_c/i_a ratio dropped to 0.78 (entry 2). Interestingly, in the presence of MeOH, the i_c/i_a ratio stayed at around 0.94 (entry 1). The drop in stability in *n*-BuOH can be rationalized by a nucleophilic attack of the alcohol on the ferrocenium cation. It appears that MeOH would not undergo such an attack, which may be somewhat counterintuitive. We speculated that MeOH nucleophile is better solvated by the CH_3CN solvent, though. In turn, in the presence of *i*-PrOH, the stability of the ferrocenium cation is also high, as reflected by an i_c/i_a ratio of 0.95 to 0.96 (entries 3 and 7). This may be a consequence of the low nucleophilicity of the secondary *i*-PrOH compared to the primary alcohol *n*-butanol.

Interestingly, the ketoferrocenophanium cation $\mathbf{1}^+$ shows in CH_3CN a lower, but consistent stability, as demonstrated by i_c/i_a ratios around 0.81 (entries 8 to 12). The ratios stay constant across different nucleophiles. Presumably, a chemical change of $\mathbf{1}^+$ takes place without the nucleophile being directly involved. The stability for different alcohol nucleophiles is slightly higher in CH_2Cl_2 (i_c/i_a ratios of 0.75 to 0.87 entries 13 to 16); here, the presence of the propargylic alcohol **3** leads to a slight decrease in stability, for which we do not have a clear explanation. Lower solvation of **3** may play a role here again.

However, the cation derived from the ferrocenophane **2** seems to be the most stable under these conditions, with average i_c/i_a ratios of 0.91 to 0.97 in CH_3CN and CH_2Cl_2 in the presence of *n*-BuOH and MeOH. It appears that the ferrocenophanium cation $\mathbf{2}^+$ is somewhat more stable than the ferrocenophanium cation $\mathbf{1}^+$ and the ferrocenium cation itself in the presence of MeOH and *n*-BuOH.

A possible explanation may be that the alkyl bridge in **2** protects the complex from bimolecular decomposition, assuming that the decomposition process involves the attack of *n*-BuOH on the iron center. The slightly more extended decomposition of the ferrocenium cation in the presence of *n*-BuOH may be due to the lack of the protecting bridge, facilitating the attack on the iron center. The ketoferrocenophanium complex $\mathbf{1}^+$ seems overall to be somewhat less stable than the ferrocenophanium cation $\mathbf{2}^+$. Here, the electron-withdrawing keto group on the Cp ring may make the iron center more electrophilic, facilitating an attack of the alcohol on the iron center, despite some protection from the bridge. Also, involvement of the carbonyl group in the decomposition process, for example, through the formation of a hemiacetal, may play a role.

We also performed the experiments in Table 3 at different sweep rates, and for ferrocene and ferrocenophane **1** in presence of *n*-BuOH, the results are compiled in Table 4. Here, for ferrocene, a clear dependency of the sweep rate on the i_c/i_a ratios can be observed in CH_3CN. The i_c/i_a ratios increase with increasing sweep rate. At a slower sweep rate, the ferrocenium ion is exposed for a longer time to the *n*-BuOH nucleophile, resulting in decomposition to a larger extent, which leads to lower i_c/i_a ratios. The i_c/i_a ratios for the ferrocenophanes **1** and **2** are relatively independent of the sweep rate with the exception of ketoferrocenophane **1**, where the i_c/i_a ratio decreases with increasing sweep rate in CH_2Cl_2. It may be speculated that for $\mathbf{1}^+$ and $\mathbf{2}^+$, decomposition by a nucleophilic attack is, within the timeframe of the CV experiment, diminished due to the protecting bridge in the ferrocenophanes.

Table 4. i_c/i_a values at different sweep rates in the presence of *n*-BuOH.

Entry	Sweep Rate mV/s	i_c/i_a Ferrocene and *n*-BuOH		i_c/i_a Ketoferroceno-phane 1 and *n*-BuOH		i_c/i_a Ferroceno-phane 2 and *n*-BuOH	
		CH_3CN	CH_2Cl_2	CH_3CN	CH_2Cl_2	CH_3CN	CH_2Cl_2
1	50	55 ± 4	92 ± 4	90 ± 2	83 ± 2	92 ± 6	95 ± 2
2	100	71 ± 5	95 ± 2	92 ± 4	83 ± 3	96 ± 2	91 ± 2
3	200	66 ± 6	92 ± 2	90 ± 2	79 ± 5	92 ± 6	88 ± 1
4	300	71 ± 2	90 ± 2	91 ± 4	77 ± 6	95 ± 4	87 ± 2
5	400	77 ± 4	90 ± 3	91 ± 6	75 ± 5	96 ± 2	86 ± 4
6	500	78 ± 3	89 ± 3	91 ± 2	70 ± 6	96 ± 2	91 ± 2

Conditions: glassy carbon working electrode, Pt counter electrode, Ag wire pseudoreference electrode at a scan rate of 100 mV s^{-1}. Solutions 1 mM in the substrate, 0.1 M in *n*-Bu_4NPF_6 and flushed with argon in presence of *n*-BuOH (0.5 mL).

The results in Tables 2–4 are of interest in several respects. The bridges in the ferrocenophanes provide some protection for their respective cations in solution, and the protecting effect seems to be dependent on the solvent and the type of the nucleophile. However, the trend is less pronounced than expected. Ferrocene seems to be slightly more stable under the conditions in Table 3 than the ketoferrocenophane **1**. It appears that the ferrocenium cation decomposes faster in the presence of *n*-BuOH, so the bridge in **1** may provide some protection over extended periods of time. In some instances, the decomposition increases with decreasing sweep rate. The findings may have some mechanistic impacts. We assume for the propargylic substitution reaction in Scheme 1 (bottom) an ionic mechanism, where first a propargylic carbocation is generated, which then can be attacked by the alcohol nucleophile [46]. The ferrocenium or ferrocenophanium cations to be applied for chemistry like in Scheme 1 (bottom) may undergo a chemical change substantially in the presence of *n*-butanol prior to or during catalysis.

2.2. Catalytic Experiments

In order to find out whether the catalyst stability has an impact on the activity, we employed the $\mathbf{1}^+SbF_6$ and $\mathbf{2}^+SbF_6$ in the propargylic test reaction in Scheme 1 (bottom) and two more reactions and compared them to the efficiency of the ferrocenium cation previously established in our research group. The results are compiled in Table 5. The reaction of the propargylic alcohol **3** with *n*-BuOH gave previously the propargylic ether product **5** [47]. The propargylic substitution reaction of the cyclopropyl-substituted propargylic alcohol **6** also resulted previously in the ring-opened eneyne product **7** when ferrocenium hexafluorophosphate ($FcPF_6$) was employed as a catalyst; the thiophenyl-substituted propargylic alcohol **8** gave the substitution product **9** with the cyclopropyl ring still intact [46].

Overall, the complexes $\mathbf{1}^+SbF_6$ and $\mathbf{2}^+SbF_6$ appear to be not as catalytically active as the ferrocenium cation itself. While some product was observed by GC, we were able to isolate the products in only 1 to 44% yields. The reactions in Table 5 are routine in our laboratory, and when employing $FcPF_6$, we obtain frequently yields of at least 30% and higher [46,47]. Of the alcohols employed in Table 5, propargylic alcohol **3** showed the least activity in substitution reactions in our previous experiments [46,47]. Obviously, $\mathbf{1}^+SbF_6$ and $\mathbf{2}^+SbF_6$ seem not reactive enough to activate the propargylic alcohol **3** toward substitution. The cyclopropyl-substituted propargylic alcohol **6** is activated toward nucleophilic substitution [46], and both catalysts $\mathbf{1}^+SbF_6$ and $\mathbf{2}^+SbF_6$ result in moderate yields for the formation of eneyne **7**. The thiophenyl-substituted propargylic alcohol **8** is also activated toward nucleophilic substitution [46]; however, both catalysts gave no detectable product **9** or only very little of it. The yield of **7** is slightly higher for $\mathbf{2}^+$; however, the general trend points toward a lower catalytic activity.

Table 5. Catalysis results.

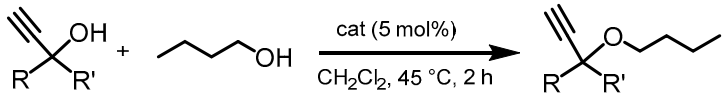

Substrate	Product [1]	Isolated Yield Fc^+	Isolated Yield 1^+	Isolated Yield 2^+
	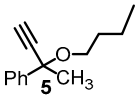	74% [2]	0%	0%
	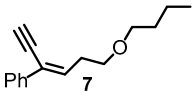	37% [3]	13%	44%
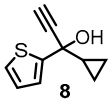	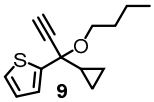	44% [3]	-	6%

[1] Reaction conditions: propargylic alcohol and alcohol in an equimolar amount, CH_2Cl_2 solvent at 45 °C for 2 h followed by chromatographic workup; [2] Data taken from [47]. [3] Data taken from [46].

The low yields in Table 5 for the ferrocenophanium complexes may indicate that the somewhat increased stability of the complexes decreases their activity. Catalysts must exhibit a level of reactivity in order to show catalytic activity. Another point to be considered is the actual catalytically active species when $FcPF_6$ is employed as a catalyst. While the ferrocenium cation may show some stability under cyclic voltammetry conditions (room temperature and short reaction time), it may undergo chemical changes under the catalytic conditions in Table 5 (45 °C and at least 2 h reaction time). Longer reaction times with ketoferrocenophanium complex $\mathbf{1}^+$ did not result in higher yields, though. Whether the decomposition products of the ferrocenium or ferrocenophanium cations are the actual catalytically active species is currently under investigation in our research group. If the ferrocenophanium complexes show somewhat increased stability in solution, as hypothesized, the reactivity may just be lower.

3. Conclusions

Overall, cyclic voltammetry data presented herein establish a moderate protecting effect of the bridge in ferrocenophanium cations in presence of alcohol nucleophiles compared to ferrocenium. These findings were established by CV i_c/i_a values and their dependency on the sweep rate. However, catalytic experiments revealed that the ferrocenophanium cations showed overall lower catalytic activity compared to the ferrocenium cation, as judged by lower isolated catalysis product yields. While decreased catalytic stability may result in decreased catalytic activity, very reactive catalysts in solution may also show a higher tendency to decompose. The catalytic activity landscape of ferrocenium and ferrocenophanium cations investigated herein may be more complex than it appears at first glance.

Supplementary Materials: The following are available online at https://www.mdpi.com/article/10.3390/molecules28062729/s1, Synthetic procedures, Figure S1: Part of the crystal structure of $\mathbf{1}^+SbF_6$, Figure S2: Molecular packing of the crystal, Table S1: Intermolecular interaction geometries of $\mathbf{1}^+SbF_6$, plot of the i_{max} value vs the square root of the scan rates, IR and UV-vis spectra of $\mathbf{1}^+SbF_6$ and $\mathbf{2}^+SbF_6$, NMR spectra of catalysis products [95–101].

Author Contributions: Conceptualization, E.B.B.; methodology, S.A.B., N.U.; investigation, S.A.B., N.U., C.W., M.B.-F., R.J.; data curation, R.J.; writing—original draft preparation, E.B.B.; writing—review and editing, S.A.B., N.U., C.W., M.B.-F., R.J.; visualization, S.A.B., E.B.B.; funding acquisition, E.B.B. All authors have read and agreed to the published version of the manuscript.

Funding: Support of this research by funds from the Banavali Green and Sustainable Chemistry Fund in Arts and Science at the University of Missouri – Saint Louis is gratefully acknowledged. The Office of the Vice Chancellor for Research and Economic & Community Development at UMSL is also gratefully acknowledged for support.

Institutional Review Board Statement: Not applicable.

Informed Consent Statement: Not applicable.

Data Availability Statement: The CIF file of the finalized crystal structure $\mathbf{1}^{+}SbF_6$ has been deposited in the Cambridge Structural Database and the reference ID is CCDC 2184543.

Conflicts of Interest: The authors declare no conflict of interest.

References

1. Gandeepan, P.; Müller, T.; Zell, D.; Cera, G.; Warratz, S.; Ackermann, L. 3d Transition Metals for C–H Activation. *Chem. Rev.* **2019**, *119*, 2192–2452. [CrossRef] [PubMed]
2. Fürstner, A. Iron Catalyzed C–C-Bond Formation: From Canonical Cross Coupling to a Quest for New Reactivity. *Bull. Chem. Soc. Jpn.* **2021**, *94*, 666–677. [CrossRef]
3. Rana, S.; Biswas, J.P.; Paul, S.; Paika, A.; Maiti, D. Organic synthesis with the most abundant transition metal–iron: From rust to multitasking catalysts. *Chem. Soc. Rev.* **2021**, *50*, 243–472. [CrossRef] [PubMed]
4. Bisz, E. Iron-Catalyzed Cross-Coupling Reactions of Alkyl Grignards with Aryl Chlorobenzenesulfonates. *Molecules* **2021**, *26*, 5895. [CrossRef]
5. Wei, D.; Netkaew, C.; Darcel, C. Multi-Step Reactions Involving Iron-Catalysed Reduction and Hydrogen Borrowing Reactions. *Eur. J. Inorg. Chem.* **2019**, 2471–2487. [CrossRef]
6. Wei, D.; Darcel, C. Iron Catalysis in Reduction and Hydrometalation Reactions. *Chem. Rev.* **2019**, *119*, 2550–2610. [CrossRef]
7. Piontek, A.; Bisz, E.; Szostak, M. Iron-Catalyzed Cross-Couplings in the Synthesis of Pharmaceuticals: In Pursuit of Sustainability. *Angew. Chem. Int. Ed.* **2018**, *57*, 11116–11128. [CrossRef]
8. Fürstner, A. Iron Catalysis in Organic Synthesis: A Critical Assessment of What It Takes to Make This Base Metal a Multitasking Champion. *ACS Cent. Sci.* **2016**, *2*, 778–789. [CrossRef]
9. Bauer, I.; Knölker, H.J. Iron catalysis in organic synthesis. *Chem. Rev.* **2015**, *115*, 3170–3387. [CrossRef]
10. Bauer, E.B. (Ed.) *Iron Catalysis II.*; Springer: New York, NY, USA, 2015.
11. Mihovilovic, D.; Schnürch, M. Ligand-Assisted Iron Catalysis in the Direct Functionalization of C–H Bonds. *ChemCatChem* **2014**, *6*, 2194–2196. [CrossRef]
12. Gopalaiah, K. Chiral iron catalysts for asymmetric synthesis. *Chem. Rev.* **2013**, *113*, 3248–3296. [CrossRef]
13. MacLeod, K.C.; Holland, P.L. Recent developments in the homogeneous reduction of dinitrogen by molybdenum and iron. *Nat. Chem.* **2013**, *5*, 559–565. [CrossRef]
14. Welcher, A.; Jacobi von Wangelin, A. Iron(0) Nanoparticle Catalysts in Organic Synthesis. *Curr. Org. Chem.* **2013**, *17*, 326–355. [CrossRef]
15. Sun, X.; Li, J.; Huang, X.; Sun, C. Recent Advances in Iron-Catalyzed C-H Bond Activation Reactions. *Curr. Inorg. Chem.* **2012**, *2*, 64–85. [CrossRef]
16. Sun, C.-L.; Li, B.-J.; Shi, Z.-J. Direct C− H transformation via iron catalysis. *Chem. Rev.* **2011**, *111*, 1293–1314. [CrossRef]
17. Sarhan, A.A.O.; Bolm, C. Iron (III) chloride in oxidative C–C coupling reactions. *Chem. Soc. Rev.* **2009**, *38*, 2730–2744. [CrossRef]
18. Lee, H.; He, T.; Cook, S.P. Iron-Catalyzed, Directed Benzylic Borylation. *Org. Lett.* **2023**, *25*, 1–4. [CrossRef]
19. Xu, H.; Li, M.-J.; Chen, H.; Huang, F.-H.; Zhu, Q.-Y.; Wang, G.-W.; Zhang, Z. $I_2/FeCl_3$-Catalyzed Domino Reaction of Aurones with Enamino Esters for the Synthesis of Highly Functionalized Pyrroles. *Org. Lett.* **2022**, *24*, 8406–8411. [CrossRef]
20. He, C.; Ma, F.; Zhang, W.; Tong, R. Reinvestigating $FeBr_3$-Catalyzed Alcohol Oxidation with H_2O_2: Is a High-Valent Iron Species (HIS) or a Reactive Brominating Species (RBS) Responsible for Alcohol Oxidation? *Org. Lett.* **2022**, *24*, 3499–3503. [CrossRef]
21. Lu, H.; Zhou, C.; Wang, Z.; Kato, T.; Liu, Y.; Maruoka, K. Fe-Catalyzed Three-Component Coupling Reaction of α, β, γ, δ-Unsaturated Carbonyl Compounds and Conjugate Dienes with Alkylsilyl Peroxides and Nucleophiles. J. *Org. Chem.* **2022**, *87*, 8824–8834. [CrossRef]
22. Qiu, Y.-F.; Chen, S.-P.; Cao, J.-H.; Li, M.; Quan, Z.-J.; Wang, X.-C.; Liang, Y.-M. Iron(II)-Catalyzed Bisphosphorylation Cascade Cycloisomerization of γ-Hydroxyl Ynones and Diphenylphosphine Oxides: Synthesis of Highly Substituted Bisphosphorylated Dihydrofuran Derivatives. *Org. Lett.* **2022**, *24*, 2264–2268. [CrossRef] [PubMed]
23. Kong, W.-J.; Kessler, S.N.; Wu, H.; Bäckvall, J.-E. Iron-Catalyzed Cross-Coupling of α-Allenyl Esters with Grignard Reagents for the Synthesis of 1,3-Dienes. *Org. Lett.* **2023**, *25*, 120–124. [CrossRef] [PubMed]
24. Zhang, Y.; Qian, J.; Wang, M.; Huang, Y.; Hu, P. Visible-Light-Induced Decarboxylative Fluorination of Aliphatic Carboxylic Acids Catalyzed by Iron. *Org. Lett.* **2022**, *24*, 5972–5976. [CrossRef] [PubMed]
25. Bisz, E.; Szostak, M. Iron-Catalyzed $C(sp^2)$–$C(sp^3)$ Cross-Coupling of Aryl Chlorobenzoates with Alkyl Grignard Reagents. *Molecules* **2020**, *25*, 230. [CrossRef] [PubMed]

26. Das, S.; Wendt, B.; Möller, K.; Junge, K.; Beller, M. Two iron catalysts are better than one: A general and convenient reduction of aromatic and aliphatic primary amides. *Angew. Chem. Int. Ed.* **2012**, *51*, 1662–1666. [CrossRef]
27. Zhang, X.; Li, Y. Light-Induced Iron-Catalyzed Trifluoromethylative Thiolation of Alkenes. *Org. Lett.* **2022**, *24*, 8057–8061. [CrossRef]
28. Emayavaramban, B.; Chakraborty, P.; Dahiya, P.; Sundararaju, B. Iron-Catalyzed α-Methylation of Ketones Using Methanol as the C1 Source under Photoirradiation. *Org. Lett.* **2022**, *24*, 6219–6223. [CrossRef]
29. Gudmundsson, A.; Schlipköter, K.E.; Bäckvall, J.-E. Iron (II)-Catalyzed Biomimetic Aerobic Oxidation of Alcohols. *Angew. Chem. Int. Ed.* **2020**, *59*, 5403–5406. [CrossRef]
30. Iwamoto, T.; Okuzono, C.; Adak, L.; Jin, M.; Nakamura, M. Iron-catalysed enantioselective Suzuki–Miyaura coupling of racemic alkyl bromides. *Chem. Commun.* **2019**, *55*, 1128–1131. [CrossRef]
31. Vicens, L.; Olivo, G.; Costas, M. Rational design of bioinspired catalysts for selective oxidations. *ACS Catal.* **2020**, *10*, 8611–8631. [CrossRef]
32. Gérard, E.F.; Yadav, V.; Goldberg, D.P.; de Visser, S.P. What Drives Radical Halogenation versus Hydroxylation in Mononuclear Nonheme Iron Complexes? A Combined Experimental and Computational Study. *J. Am. Chem. Soc.* **2022**, *144*, 10752–10767. [CrossRef]
33. Olivo, G.; Capocasa, G.; Ticconi, B.; Lanzalunga, O.; Di Stefano, S.; Costas, M. Predictable selectivity in remote C− H oxidation of steroids: Analysis of substrate binding mode. *Angew. Chem. Int. Ed* **2020**, *59*, 12703–12708. [CrossRef]
34. Olivo, G.; Capocasa, G.; Lanzalunga, O.; Di Stefano, S.; Costas, M. Enzyme-like substrate-selectivity in C–H oxidation enabled by recognition. *Chem. Commun.* **2019**, *55*, 917–920. [CrossRef]
35. Olivo, G.; Farinelli, G.; Barbieri, A.; Lanzalunga, O.; Di Stefano, S.; Costas, M. Supramolecular Recognition Allows Remote, Site-Selective C− H Oxidation of Methylenic Sites in Linear Amines. *Angew. Chem. Int. Ed.* **2017**, *129*, 16565–16569. [CrossRef]
36. Lauzon, S.; Schouwey, L.; Ollevier, T. C_2-Symmetric 2,2′-Bipyridine-α,α′-1-adamantyl-diol Ligand: Bulky Iron Complexes in Asymmetric Catalysis. *Org. Lett.* **2022**, *24*, 1116–1120. [CrossRef]
37. Pellissier, H. Recent developments in enantioselective iron-catalyzed transformations. *Coord. Chem. Rev.* **2019**, *386*, 1–31. [CrossRef]
38. Ollevier, T. Iron bis(oxazoline) complexes in asymmetric catalysis. *Catal. Sci. Technol.* **2016**, *6*, 41–48. [CrossRef]
39. Lenze, M.; Bauer, E.B. Chemoselective, iron (II)-catalyzed oxidation of a variety of secondary alcohols over primary alcohols utilizing H_2O_2 as the oxidant. *Chem. Commun.* **2013**, *49*, 5889–5891. [CrossRef]
40. Lenze, M.; Martin, E.T.; Rath, N.P.; Bauer, E.B. Iron (II) α-Aminopyridine Complexes and Their Catalytic Activity in Oxidation Reactions: A Comparative Study of Activity and Ligand Decomposition. *ChemPlusChem* **2013**, *78*, 101–116. [CrossRef]
41. Lenze, M.; Sedinkin, S.L.; Bauer, E.B. Polydentate pyridyl ligands and the catalytic activity of their iron (II) complexes in oxidation reactions utilizing peroxides as the oxidants. J. *Mol. Catal. A* **2013**, *373*, 161–171. [CrossRef]
42. Shejwalkar, P.; Rath, N.P.; Bauer, E.B. New iron (II) α-iminopyridine complexes and their catalytic activity in the oxidation of activated methylene groups and secondary alcohols to ketones. *Dalton Trans.* **2011**, *40*, 7617–7631. [CrossRef] [PubMed]
43. Shejwalkar, P.; Rath, N.P.; Bauer, E.B. New chiral phosphoramidite complexes of iron as catalytic precursors in the oxidation of activated methylene groups. *Molecules* **2010**, *15*, 2631–2650. [CrossRef] [PubMed]
44. Lenze, M.; Sedinkin, S.L.; Rath, N.P.; Bauer, E.B. New indenyl phosphinooxazoline complexes of iron and their catalytic activity in the Mukaiyama aldol reaction. *Tetrahedron Lett.* **2010**, *51*, 2855–2858. [CrossRef]
45. Lenze, M.; Bauer, E.B. Oxidation of activated methylene groups to ketones catalyzed by new iron phosphinooxazoline complexes and by iron (II) triflate. *J. Mol. Catal. A* **2009**, *309*, 117–123. [CrossRef]
46. Talasila, D.S.; Queensen, M.J.; Barnes-Flaspoler, M.; Jurkowski, K.; Stephenson, E.; Rabus, J.M.; Bauer, E.B. Ferrocenium Cations as Catalysts for the Etherification of Cyclopropyl-Substituted Propargylic Alcohols: Ene-yne Formation and Mechanistic Insights. *Eur. J. Org. Chem.* **2019**, *2019*, 7348–7358. [CrossRef]
47. Queensen, M.Q.; Rabus, J.M.; Bauer, E.B. Ferrocenium hexafluorophosphate as an inexpensive, mild catalyst for the etherification of propargylic alcohols. *J. Mol. Cat. A: Chem* **2015**, *407*, 221–229. [CrossRef]
48. Toma, Š.; Šebesta, R. Applications of ferrocenium salts in organic synthesis. *Synthesis* **2015**, *47*, 1683–1695. [CrossRef]
49. Ang, H.T.; Rygus, J.P.G.; Hall, D.G. Two-component boronic acid catalysis for increased reactivity in challenging Friedel–Crafts alkylations with deactivated benzylic alcohols. *Org. Biomol. Chem.* **2019**, *17*, 6007–6014. [CrossRef]
50. Mo, X.; Yakiwchuk, J.; Dansereau, J.; McCubbin, J.A.; Hall, D.G. Unsymmetrical Diarylmethanes by Ferroceniumboronic Acid Catalyzed Direct Friedel–Crafts Reactions with Deactivated Benzylic Alcohols: Enhanced Reactivity due to Ion-Pairing Effects. *J. Am. Chem. Soc.* **2015**, *137*, 9694–9703. [CrossRef]
51. Mo, X.; Hall, D.G. Dual catalysis using boronic acid and chiral amine: Acyclic quaternary carbons via enantioselective alkylation of branched aldehydes with allylic alcohols. *J. Am. Chem. Soc.* **2016**, *138*, 10762–10765. [CrossRef]
52. Deb, M.; Hazra, S.; Dolui, P.; Elias, A.J. Ferrocenium Promoted Oxidation of Benzyl Amines to Imines Using Water as the Solvent and Air as the Oxidant. *ACS Sustainable Chem. Eng.* **2019**, *7*, 479–486. [CrossRef]
53. Shul'pina, L.S.; Kudinov, A.R.; Mandelli, D.; Carvalho, W.A.; Kozlov, Y.N.; Vinogradov, M.M.; Ikonnikov, N.S.; Shul'pin, G.B. Oxidation of alkanes and benzene with hydrogen peroxide catalyzed by ferrocene in the presence of acids. *J. Organomet. Chem.* **2015**, *793*, 217–231. [CrossRef]

54. Khan, N.-u.H.; Agrawal, S.; Kureshy, R.I.; Abdi, S.H.R.; Singh, S.; Jasra, R.V. $Fe(Cp)_2PF_6$: An efficient catalyst for cyanosilylation of carbonyl compounds under solvent free condition. *J. Organomet. Chem.* **2007**, *692*, 4361–4366. [CrossRef]
55. Argouarch, G.; Grelaud, G.; Roisnel, T.; Humphrey, M.G.; Paul, F. [Fp*Fc][PF_6]: A remarkable non-symmetric dinuclear cation in a very stable mixed-valent state. *J. Organomet. Chem.* **2017**, *847*, 218–223. [CrossRef]
56. Yadav, G.D.; Chauhan, M.M.S.; Singh, S. $Fe(Cp)_2BF_4$: An efficient Lewis acid catalyst for the aminolysis of epoxides. *Synthesis* **2014**, *46*, 629–634.
57. Yadav, G.D.; Singh, S. Ring opening of epoxides with alcohols using $Fe(Cp)_2BF_4$ as catalyst. *Tetrahedron Lett.* **2014**, *55*, 3979–3983. [CrossRef]
58. Mukaiyama, T.; Kitagawa, H.; Matsuo, J.-i. Aromatic iodination with iodine monochloride by using a catalytic amount of ferrocenium tetrakis (3, 5-bis (trifluoromethyl) phenyl) borate. *Tetrahedron Lett.* **2000**, *41*, 9383–9386. [CrossRef]
59. Noor-ul, K.H.; Agrawal, S.; Kureshy, R.I.; Abdi, S.H.R.; Singh, S.; Suresh, E.; Jasra, R.V. $Fe(Cp)_2PF_6$ catalyzed efficient Strecker reactions of ketones and aldehydes under solvent-free conditions. *Tetrahedron Lett.* **2008**, *49*, 640–644.
60. Kureshy, R.I.; Agrawal, S.; Saravanan, S.; Khan, N.-u.H.; Shah, A.K.; Abdi, S.H.R.; Bajaj, H.C.; Suresh, E. Direct Mannich reaction mediated by $Fe(Cp)_2PF_6$ under solvent-free conditions. *Tetrahedron Lett.* **2010**, *51*, 489–494. [CrossRef]
61. Peña, L.A.; Seidl, A.J.; Cohen, L.R.; Hoggard, P.E. Ferrocene/ferrocenium ion as a catalyst for the photodecomposition of chloroform. *Transition Met. Chem.* **2009**, *34*, 135–141. [CrossRef]
62. Neumann, A.; Prehn Junquera, A.; Wismach, C.; Jones, P.G.; Streubel, R. Synthesis of functional Δ3-1,3,5-oxazaphospholene and 2H-1,4,2-diazaphosphole complexes via catalytic ring expansion reactions of a 2H-azaphosphirene complex. *Tetrahedron* **2003**, *59*, 6213–6220. [CrossRef]
63. Zhang, J.; Campolo, C.; Dumur, F.; Xiao, P.; Gigmes, D.; Fouassier, J.P.; Lalevée, J. The carbazole-bound ferrocenium salt as a specific cationic photoinitiator upon near-UV and visible LEDs (365–405 nm). *Polym. Bull.* **2016**, *73*, 493–507. [CrossRef]
64. Li, M.; Chen, Y.; Zhang, H.; Wang, T. A novel ferrocenium salt as visible light photoinitiator for cationic and radical photopolymerization. *Prog. Org. Coat.* **2010**, *68*, 234–239. [CrossRef]
65. Wang, T.; Chen, J.W.; Li, Z.Q.; Wan, P.Y. Several ferrocenium salts as efficient photoinitiators and thermal initiators for cationic epoxy polymerization. *J. Photochem. Photobiol. A Chem.* **2007**, *187*, 389–394. [CrossRef]
66. Wang, T.; Li, B.S.; Zhang, L.X. Carbazole-bound ferrocenium salt as an efficient cationic photoinitiator for epoxy polymerization. *Polym. Int.* **2005**, *54*, 1251–1255. [CrossRef]
67. Görmen, M.; Pigeon, P.; Hillard, E.A.; Vessières, A.; Huché, M.; Richard, M.-A.; McGlinchey, M.J.; Top, S.; Jaouen, G. Synthesis and antiproliferative effects of [3] ferrocenophane transposition products and pinacols obtained from McMurry cross-coupling reactions. *Organometallics* **2012**, *31*, 5856–5866. [CrossRef]
68. Singh, A.; Roy Chowdhury, D.; Paul, A. A kinetic study of ferrocenium cation decomposition utilizing an integrated electrochemical methodology composed of cyclic voltammetry and amperometry. *Analyst* **2014**, *139*, 5747–5754. [CrossRef]
69. Prins, R.; Korswagen, A.R.; Kortbeek, A.G.T.G. Decomposition of the ferricenium cation by nucleophilic reagents. *J. Organomet. Chem.* **1972**, *39*, 335–344. [CrossRef]
70. Zotti, G.; Schiavon, G.; Zecchin, S.; Favretto, D. Dioxygen-decomposition of ferrocenium molecules in acetonitrile: The nature of the electrode-fouling films during ferrocene electrochemistry. *J. Electroanal. Chem.* **1998**, *456*, 217–221. [CrossRef]
71. Hurvois, J.P.; Moinet, C. Reactivity of ferrocenium cations with molecular oxygen in polar organic solvents: Decomposition, redox reactions and stabilization. *J. Organomet. Chem.* **2005**, *690*, 1829–1839. [CrossRef]
72. Lorans, J.; Pierre, F.; Toupet, L.; Moinet, C. Anodic co-oxidation of urazole and ferrocenes: First trapping ofcyclopentadienols. *Chem. Commun.* **1997**, 1279–1280. [CrossRef]
73. Allen, S.K.; Lathrop, T.E.; Patel, S.B.; Harrell Moody, D.M.; Sommer, R.D.; Coombs, T.C. Synthesis of 7-norbornenols via Diels–Alder cycloadditions of cyclopentadienol generated by decomposition of ferrocenium cation. *Tetrahedron Lett.* **2015**, *56*, 6038–6042. [CrossRef]
74. Heo, R.W.; Randall Lee, T. Ferrocenophanes with all carbon bridges. *J. Organomet. Chem.* **1999**, *578*, 31–42. [CrossRef]
75. Aggarwal, V.K.; Jones, D.; Turner, M.L.; Adams, H. First synthesis and X-ray crystal structure of 1, 2-(1, 1′-ferrocenediyl) ethene. *J. Organomet. Chem.* **1996**, *524*, 263–266. [CrossRef]
76. Werner, I.; Heinisch, S.L.; Nowik, I.; Herber, R.H.; Butenschön, H. 1,16-Di-*tert*-butyl-1,16-diphospha[5.5]ferrocenophane: Synthesis, Reactions and Mössbauer Spectroscopy. *ChemistrySelect* **2018**, *3*, 13132–13139. [CrossRef]
77. Braunschweig, H.; Krummenacher, I.; Lichtenberg, C.; Mattock, J.D.; Schäfer, M.; Schmidt, U.; Schneider, C.; Steffenhagen, T.; Ullrich, S.; Vargas, A. Dibora[2]ferrocenophane: A Carbene-Stabilized Diborene in a Strained cis-Configuration. *Angew. Chem. Int. Ed.* **2017**, *56*, 889–892. [CrossRef]
78. Buchowicz, W.; Guńka, P.A.; Buchalski, P.; Piszcz, M.; Buś, S.; Mrozowicz, M.; Mazur, M.; Wasilewski, R. *E*/*Z* Switchable Ring-Closing Metathesis in 1,1′-Bis(but-3-enyl)ferrocenes: Synthesis and Characterization of Axially Chiral ansa[6]-Ferrocenes. *Organometallics* **2022**, *41*, 1968–1976. [CrossRef]
79. Musgrave, R.A.; Russell, A.D.; Manners, I. Strained ferrocenophanes. *Organometallics* **2013**, *32*, 5654–5667. [CrossRef]
80. Turbitt, T.D.; Watts, W.E. Bridged ferrocenes: XII. The synthesis of [3] ferrocenophan-1-one from ferrocene by a novel one-step annelation reaction. *J. Organomet. Chem.* **1972**, *46*, 109–117. [CrossRef]
81. Dong, T.-Y.; Lee, S.-H. The effects of an interannular bridge on the electronic structure of ferrocenium cations. *J. Organomet. Chem.* **1995**, *487*, 77–88. [CrossRef]

82. Carty, P.; Dove, M.F.A. The reaction of some ferrocenyl ketones with anhydrous silver tetrafluoroborate, a new route to substituted ferricenium salts. *J. Organomet. Chem.* **1971**, *28*, 125–132. [CrossRef]
83. Watanabe, M.; Sato, K.; Motoyama, I.; Sano, H. Mössbauer Studies of Bridged Ferrocenophane Derivative's Polyiodides. *Chemistry Letters* **1983**, *12*, 1775–1778. [CrossRef]
84. Duggani, D.M.; Hendrickson, D.N. Electronic structure of various ferricenium systems as inferred from Raman, infrared, low-temperature electronic absorption, and electron paramagnetic resonance measurements. *Inorg. Chem.* **1975**, *14*, 955–970. [CrossRef]
85. Khozeimeh Sarbisheh, E.; Bhattacharjee, H.; Cao, M.P.T.; Zhu, J.; Müller, J. How strained are [1] ferrocenophanes? *Organometallics* **2017**, *36*, 614–621. [CrossRef]
86. Althoff, A.; Jutzi, P.; Lenze, N.; Neumann, B.; Stammler, A.; Stammler, H.-G. A Digalla[1.1]ferrocenophane and Its Coordination Chemistry: Synthesis and Structure of $[\{Fe(\eta^5\text{-}C_5H_4)_2\}_2\{GaMe\}_2]$ and of the Adducts $[\{Fe(\eta^5\text{-}C_5H_4)_2\}_2\{GaMe(D)\}_2]$ (D = Monodentate Donor) and $[\{Fe(\eta^5\text{-}C_5H_4)_2\}_2\{GaMe\}_2D]$ (D = Bidentate Donor). *Organometallics* **2003**, *22*, 2766–2774. [CrossRef]
87. Bhattacharjee, H.; Dey, S.; Zhu, J.; Sun, W.; Müller, J. Strained azabora [2] ferrocenophanes. *Chem. Commun.* **2018**, *54*, 5562–5565. [CrossRef]
88. Herbert, D.E.; Mayer, U.F.J.; Manners, I. Strained Metallocenophanes and Related Organometallic Rings Containing π-Hydrocarbon Ligands and Transition-Metal Centers. *Angew. Chem. Int. Ed.* **2007**, *46*, 5060–5081. [CrossRef]
89. Reichert, A.; Bolte, M.; Lerner, H.-W.; Wagner, M. Mono- and di-borylated [3]ferrocenophanes. *J. Organomet. Chem.* **2013**, *744*, 15–23. [CrossRef]
90. Connelly, N.G.; Geiger, W.E. Chemical redox agents for organometallic chemistry. *Chem. Rev.* **1996**, *96*, 877–910. [CrossRef]
91. Elgrishi, N.; Rountree, K.J.; McCarthy, B.D.; Rountree, E.S.; Eisenhart, T.T.; Dempsey, J.L. A practical beginner's guide to cyclic voltammetry. *J. Chem. Educ.* **2018**, *95*, 197–206. [CrossRef]
92. Korb, M.; Lehrich, S.W.; Lang, H. Reactivity of ferrocenyl Phosphates bearing (hetero-) aromatics and [3] ferrocenophanes toward anionic phospho-fries rearrangements. *J. Org. Chem.* **2017**, *82*, 3102–3124. [CrossRef]
93. Frenzel, P.; Lehrich, S.W.; Korb, M.; Hildebrandt, A.; Lang, H. Ferrocenyloxysilanes: Synthesis, characterization and electrochemical investigations. *J. Organomet. Chem.* **2017**, *845*, 98–106. [CrossRef]
94. Plażuk, D.; Vessiéres, A.; Hillard, E.A.; Buriez, O.; Labbé, E.; Pigeon, P.; Plamont, M.-A.; Amatore, C.; Zakrzewski, J.; Jaouen, G. A [3] ferrocenophane polyphenol showing a remarkable antiproliferative activity on breast and prostate cancer cell lines. *J. Med. Chem.* **2009**, *52*, 4964–4967. [CrossRef]
95. Rao, W.; Zhang, X.; Sze, E.M.L.; Chan, P.W.H. Ytterbium(III) Triflate-Catalyzed Amination of 1-Cyclopropylprop-2-yn-1-ols as an Expedient Route to Conjugated Enynes. *J. Org. Chem.* **2009**, *74*, 1740–1743. [CrossRef]
96. Yamauchi, Y.; Onodera, G.; Sakata, K.; Yuki, M.; Miyake, Y.; Uemura, S.; Nishibayashi, Y. Ruthenium-Catalyzed Reactions of 1-Cyclopropyl-2-propyn-1-ols with Anilines and Water via Allenylidene Intermediates: Selective Preparation of Tri- and Tetrasubstituted Conjugated Enynes. *J. Am. Chem. Soc.* **2007**, *129*, 5175–5179. [CrossRef]
97. Bruker. *APEX3, SAINT-Plus and SADABS*; Bruker AXS Inc.: Madison, WC, USA, 2016.
98. Sheldrick, G.M. Crystal structure refinement with SHELXL. *Acta. Cryst.* **2015**, *C71*, 3–8.
99. Spek, A.L. checkCIF validation ALERTS: What they mean and how to respond. *Acta Cryst.* **2020**, *E76*, 1–11. [CrossRef]
100. Dolomanov, O.V.; Bourhis, L.J.; Gildea, R.J.; Howard, J.A.K.; Puschmann, H. OLEX2: A complete structure solution, refinement and analysis program. *J. Appl. Cryst.* **2009**, *42*, 339–341. [CrossRef]
101. Macrae, C.F.; Bruno, I.J.; Chisholm, J.A.; Edgington, P.R.; McCabe, P.; Pidcock, E.; Rodriguez-Monge, L.; Taylor, R.; van de Streek, J.; Wood, P.A. Mercury 4.0: From visualization to analysis, design and prediction. *J. Appl. Crystallogr.* **2009**, *41*, 466–470. [CrossRef]